Growth of thin Ni films on GaN(0001)-(1 × 1)

V. M. Bermudez and R. Kaplan
Naval Research Laboratory, Washington, D.C. 20375-5347

M. A. Khan and J. N. Kuznia
APA Optics, Inc., 2950 N.E. 84th Lane, Blaine, Minnesota 55434
(Received 25 January 1993)

The growth and structure of Ni films, formed by *in situ* deposition on atomically clean GaN(0001)-(1×1) surfaces, have been studied using Auger, electron-energy-loss, and ultraviolet-photoemission spectroscopies, and low-energy electron diffraction. Near room temperature, a disordered film grows in a continuous, layer-by-layer mode. Annealing a thin layer at ~700–800 °C forms ordered Ni islands in registry with the GaN. The resulting Ni(111)-(1×1) surface then induces ordering during subsequent deposition of thicker Ni layers near room temperature. Chemical reaction at the interface occurs even near room temperature. The N released appears near the Ni surface, while the free Ga remains near the interface. Annealing at $T \geq 600$ °C leads to the loss of N by desorption and to extensive intermixing of Ga and Ni. Depending on annealing temperature, Ga-induced $(\sqrt{3} \times \sqrt{3})R\,30°$ or (2×2) superstructures are observed on the Ni(111) surface. A Ga metal film deposited on the Ni layer is able to combine with some of the N, escaping during high-temperature annealing, to reform a poorly ordered GaN phase.

I. INTRODUCTION

Wide-band-gap semiconductors such as AlN, GaN, and InN are currently of interest[1] in the fabrication of a variety of electronic components. In particular, GaN is useful as an optoelectronic material in light-emitting or -detecting devices and as a passivating layer on GaAs substrates. As such, the surface properties of GaN and the formation of both Ohmic and rectifying contacts with metals are important issues.

Little previous work has been published in the area of GaN surface and interface properties. Hedman and Mårtensson[2] reported Al $K\alpha$ x-ray photoemission spectroscopy (XPS) data for single-crystal GaN layers on sapphire (0001). The binding energies of various core levels and the kinetic energies of the fine structure in the Ga *LMM* Auger spectrum were obtained. The bulk valence-band density of states was found to be in good agreement with theoretical results. Carin, Deville, and Werckmann[3] presented similar results for GaN films grown by reactive sputtering. Troost *et al.*[4] reported electron-energy-loss spectra (ELS) and ultraviolet photoemission spectra (UPS) for GaAs (110) surfaces exposed to atomic N and for Ar^+-ion bombarded (0001) surfaces of crystalline GaN. DeLouise[5] and Zhu *et al.*,[6] respectively, have reported XPS data for GaN films grown on GaAs (110) by N_2^+-ion bombardment and on GaAs (100) by photochemical reaction with NH_3. Khan *et al.*[7] have recently discussed the surface characterization of crystalline GaN films grown on (0001) sapphire by chemical vapor deposition. In particular, the clean (0001)-(1×1) surface appears to be N terminated, based on Auger measurements.[7] To the best of our knowledge, the only previous work on Ni/GaN contacts is the brief report by Kopeliovich *et al.*[8] indicating that Ohmic behavior is observed

for metals with a work function of less than ~4 eV (In, Zn, Al, and Ga) while other metals (e.g., Ni) exhibit a finite barrier height.

In the present work, we have used low-energy electron diffraction (LEED), Auger electron spectroscopy (AES), ELS, and UPS to study the growth and the structure of thin Ni films on clean and well-characterized GaN (0001)-(1×1) surfaces.

II. EXPERIMENTAL DETAILS

The GaN samples were *n*-type thin films grown[7,9] on (0001) sapphire wafers. After removal from the growth apparatus, the samples were sealed in a N_2 ambient until use. Samples (~1×1 cm²) were mounted with the sapphire substrate in close contact with a slightly larger low-resistivity Si wafer and the edges held by Ta clamps. The samples were heated by resistive heating of the Si wafer, the temperature of which was measured with a calibrated infrared pyrometer. After bakeout of the ultrahigh-vacuum (UHV) chamber the samples typically showed a high-background (1×1) LEED pattern, and oxygen (and a small amount of carbon) was observed in AES. After outgassing by prolonged heating at ~900 °C, the surface was cleaned[7] by deposition of several monolayers of Ga metal *in situ* from a graphite Knudsen cell followed by annealing for a few minutes in UHV at 900–950 °C. A few cycles of this treatment reduced the coverages of C and O to below the AES detection limits (~1% and 0.5% of a monolayer, respectively) and resulted in a sharp, low-background (1×1) LEED pattern. (Appendix A describes the procedure used for estimating impurity coverages from the Auger intensities.) Heating above ~950 °C was avoided, since LEED then showed evidence of faceting.

Ni was deposited *in situ* from a resistively heated rib-

bon of 99.995% pure metal surrounded by a liquid-N_2-cooled shield. Before mounting in UHV, the Ni was etched for a few minutes in a mixture of equal volumes of nitric and acetic acids and acetone to remove gross surface contamination. During Ni deposition, at a rate of $\sim 0.5-1$ Å min^{-1}, the chamber pressure remained below 4×10^{-10} torr. The coverage was estimated using a quartz crystal oscillator (QCO) thickness monitor. A monolayer ($\Theta_{Ni} = 1$) is defined as one Ni per GaN (0001) surface atom, or 9.89×10^{14} Ni/cm^2. On this basis, a QCO thickness of 1.0 Å corresponds to $\Theta_{Ni} = 0.92$. The only impurity observed by AES after Ni deposition was molecular CO adsorbed from the UHV background. This was revealed as a very weak O KLL peak (i.e., just above the detection limit) at 510 eV which could be removed by thermal desorption. For lower Ni coverages (i.e., a few monolayers) there is indication of dissociative CO adsorption, possibly due to defects,[10] in that the O impurity is not removed by annealing. To avoid the need for ion bombardment and high-temperature annealing (which are ineffective in preparing a well-ordered and stoichiometric GaN surface), a new sample was used each time a clean GaN surface was required. All results reported here were obtained reproducibly on at least two different samples.

Auger and energy-loss data were recorded using a double-pass cylindrical mirror analyzer (CMA) in the "nonretard" first-derivative $(d[EN(E)]/dE)$ mode. For AES, a primary beam of $E_p = 3$ keV, $i_p \approx 4$ μA was used with a peak-to-peak CMA modulation of either 1 or 2 eV. For ELS, typical parameters were $E_p = 100$ eV, $i_p \approx 0.8$ μA with a 0.5-eV modulation. The ELS resolution (fullwidth at half maximum of the elastic peak) was 0.7 eV. When necessary, ELS peak energies were accurately determined from the second-derivative spectrum, in the form of $-d^2[EN(E)]/dE^2$, obtained by numerically differentiating the experimental first-derivative spectrum.

For UPS, mainly of the Ga $3d$ core level, the CMA was operated in the "retard" mode with a 25-eV pass energy (~ 0.4 eV CMA resolution). The excitation source was the 151.4-eV $M\zeta$ line of a Zr anode operated at about 9.5 kV and 175 W. The Be foil window, normally in place when using the 2042.2-eV Zr $L\alpha_{1,2}$ line, was removed to permit access to the lower-energy photons. The CMA work-function correction was determined from the Fermi-level position of a thick layer of metallic Ga deposited on the sample.

III. RESULTS AND DISCUSSION

A. AES

1. Dependence on nickel coverage

Figures 1 and 2 show representative AES data for clean GaN and for a thick, unannealed Ni layer. Here, as elsewhere in this paper, "thick" means that little or no intensity is detected from the substrate LMM transitions. The low-energy spectra, principally the ~ 50-eV Ga $M_{2,3}M_4M_4$ doublet and the 60-eV Ni $M_{2,3}VV$, are not sufficiently well separated to provide reliable line-shape
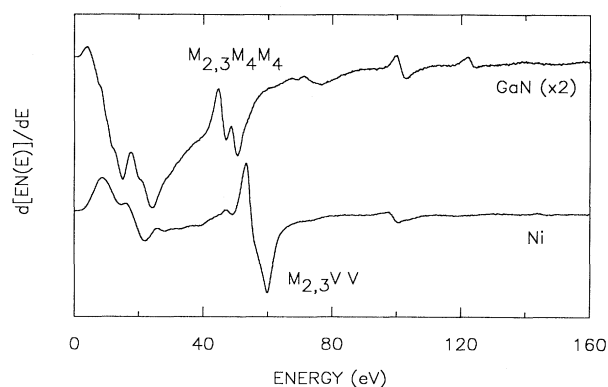

FIG. 1. Low-energy part of the Auger spectrum of clean GaN and of a thick, unannealed Ni film. The major features are the Ga $M_{2,3}M_4M_4$ and Ni $M_{2,3}VV$ transitions. The modulation amplitude was 1 eV peak to peak (pp). The GaN spectrum has been multiplied by a factor of 2, relative to that of Ni.

information in cases where intermixing occurs (see below). The N KLL fine structure, which is sensitive to differences in chemical bonding among metal nitrides,[11] is characteristic of GaN.

Figure 3 shows a plot, versus Θ_{Ni}, of a quantity derived from the 848-eV Ni LMM peak-to-peak height (PPH) for deposition at nominal room temperature (i.e., neglecting any radiative heating of the sample by the Ni source). The PPH may be affected[12] by the limited resolution at higher energies (~ 5.5 and 6.7 eV, respectively, for the main Ni and Ga LMM peaks, including the 2-eV modulation broadening). However, this effect should be independent of Θ_{Ni}. For the simple case of uniform layer-by-layer growth (i.e., a Frank–van der Merwe mechanism) one expects the expression $I_\Theta/I_\infty = 1 - \exp(-d/\lambda \cos\phi)$ to apply, where I_Θ is the PPH at a given Θ_{Ni} and I_∞ the value at "infinite" coverage. The Ni thickness in
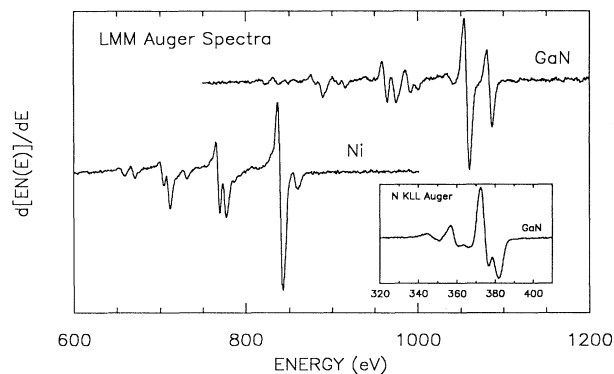

FIG. 2. High-energy parts of the Auger spectra (2-eV pp modulation) showing the Ga and Ni LMM transitions (on the same vertical scale) for clean GaN and for a thick, unannealed Ni film. The inset shows the N KLL spectrum of GaN (1-eV pp modulation).
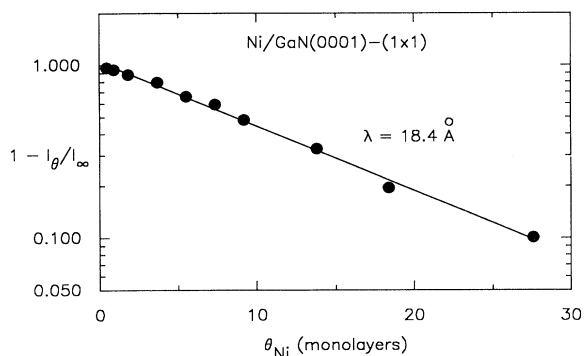
FIG. 3. Ni 848-eV LMM peak-to-peak height (PPH) vs Ni coverage, Θ_{Ni}, on GaN. The quantity plotted is $(1-I_\Theta/I_\infty)$ where I_Θ is the PPH at a given Θ_{Ni} and I_∞ the value for an "infinitely thick" layer (no Ga LMM peak visible). Fitting the data with a uniform-layer growth model (see text) gives an electron inelastic mean free path in Ni at 848 eV of $\lambda = 18.4$ Å.

angstroms is d, λ is the electron inelastic mean free path (IMFP) in Ni at 848 eV, and $\phi = 42°$ is the CMA collection angle. Fitting this equation to the data gives $\lambda \approx 18.4$ Å, somewhat higher than the semiempirical estimate of $\lambda \approx 13.2$ Å given by Tanuma, Powell, and Penn.[13] The QCO used to determine Ni coverage was not independently calibrated, and I_Θ/I_∞ may also be sensitive to long-term drift in the Auger electronics during the series of measurements. Hence the value obtained for λ in Fig. 3 may not be quantitatively accurate. However, the data are clearly consistent with layer-by-layer growth. A similar Θ_{Ni} dependence (not shown) was seen for the attenuation of the Ga 1070-eV peak, indicating the absence of extensive Ga-Ni intermixing near room temperature (see below).

2. Effects of annealing after nickel deposition

Figure 4 shows the (Ga 1070 eV)/(Ni 848 eV) PPH ratio for a series of 10-sec anneals in UHV at successively
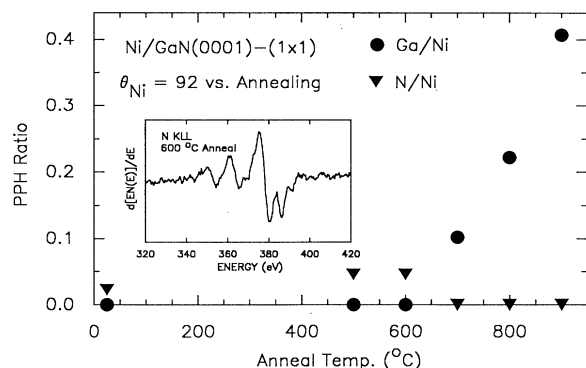
FIG. 4. (Ga 1070 eV)/(Ni 848 eV) and (N 380 eV)/(Ni 848 eV) PPH ratios vs annealing (~ 10 sec at each temperature). The initial Ni coverage is about 92 monolayers. The inset shows the N KLL spectrum (2-eV modulation) after the 600 °C anneal.

higher temperatures. Desorption of Ni is not believed to be significant under these conditions. From the vapor pressure of Ni (10^{-7} torr at 1000 °C, Ref. 14) an evaporation rate of <0.01 monolayers/sec is estimated[15] at the highest temperature used here. Simple diffusion of Ni into an otherwise undisturbed GaN lattice is also ruled out by the absence of a detectable N KLL intensity accompanying the increase in that of the Ga LMM. The weak N signal observed up to ~ 600 °C (Fig. 4) is discussed below.

Two different mechanisms can account for the effects of annealing on the PPH ratios. In one, Ni diffuses into GaN with disruption of the lattice, and free Ga and N accumulate near the surface where the latter desorbs. [Nitrogen chemisorbed on Ni (111) by exposure to atomic N desorbs[16] near 650 °C.] In the other, free Ga and N are created at the Ni/GaN interface and move to the Ni surface with no indiffusion of Ni. In either case, free Ga may also intermix[17-19] with the bulk of the Ni film. The Ni-Ga phase diagram[17] indicates that, below ~ 1200 °C, Ga is soluble in Ni up to a Ga concentration of 28 at. %. It is not possible to distinguish between these two processes with the data at hand. However, for very thick (~ 1100 Å) Ni layers on GaAs, Ogawa[18] found that the interfacial reaction occurs via Ni penetration.

3. Nitrogen desorption

During Ni deposition near room temperature, the substrate Ga LMM spectrum is attenuated to below the detection limit at a coverage of $\Theta_{Ni} \approx 45$ ($\lambda \approx 15.7$ Å in Ni at 1070 eV, Ref. 13). However, Fig. 4 indicates an observable N KLL signal at $\Theta_{Ni} \approx 90$, even though the relevant IMFP is shorter ($\lambda \approx 7.8$ Å in Ni at 380 eV). Annealing, up to the N desorption point[16] of ~ 650 °C, does not significantly affect the PPH but does sharpen the structure (Fig. 4, inset). The resulting spectrum, distinctly different from that of GaN (Fig. 2), closely resembles that of N bonded to Ni as observed[20] for N_2^+-implanted Ni(110). These results indicate that, even near room temperature, N is released by reaction at the interface between GaN and a thick Ni layer and diffuses through the film to the Ni surface.

Presumably the Ga released in the reaction initially remains near the interface since it does not appear in AES (Fig. 4) until after annealing above 600 °C. This interfacial Ga-rich layer may impede further reaction at room temperature. This would account for the fact (Fig. 4) that there is no significant increase in N KLL intensity with annealing, as would be expected if further reaction were occurring at temperatures below 600 °C. In this context, it is noteworthy that the N coverage on the Ni surface remains well below the saturation value. This is based on a comparison of the N/Ni PPH ratio in Fig. 4 with those obtained in previous studies[21,22] of N adsorption on Ni(110). Additional evidence that extensive intermixing of Ga and Ni occurs only after annealing will be seen in the Ga $3d$ UPS data discussed below.

A pressure rise was observed while annealing thick Ni layers on GaN but not for thin Ni films (i.e., a few monolayers) or for bare GaN. The threshold temperature for a

detectable pressure rise was ~600 °C, and the magnitude of the effect increased with annealing temperature. During an 800–900 °C anneal, the pressure rose to the low 10^{-8}-torr range from a base of $\leq 1 \times 10^{-10}$ torr. Gas analysis using a quadrupole mass spectrometer indicated an increase in masses 14 (N) and 28 (N_2 and/or CO). With continued heating the CO fragments at masses 12 (C) and 16 (O) appeared (due to outgassing of the sample support, heater leads, etc.) but were delayed with respect to N. This indicates that most of the initial rise in mass-28 partial pressure is due to N_2 which, presumably, originates from recombination of adsorbed N as observed[16] for N/Ni(111).

An interesting aspect of the release of N is its "recapture" by a Ga overlayer. Figure 5(a) shows AES data for a thick Ni layer after a 900 °C anneal, as in Fig. 4. No N *KLL* intensity is observed. Figure 5(b) shows the result of subsequent deposition of a thick Ga film, followed by a brief 800 °C anneal. A GaN-like N *KLL* spectrum is now seen. Further annealing, at 900–950 °C, results in an increased N *KLL* intensity and the gradual disappearance of metallic Ga. At that point, LEED (not shown) indicates a poorly ordered GaN(0001)-(1×1) surface, and the surface-sensitive ELS (not shown) resembles that of the initial, clean GaN surface. Both LEED and ELS will be discussed below. Figure 5(c) shows representative AES results obtained after extensive annealing. Thus the Ga metal overlayer is able to combine with some of the N released by the Ni/GaN reaction to regenerate a GaN layer. Since sputter profiling was not performed, the state of the Ni layer corresponding to Fig. 5(c) has not been determined. Presumably, intermixing with the GaN is complete since much milder anneals (Fig. 4) lead to extensive reaction.
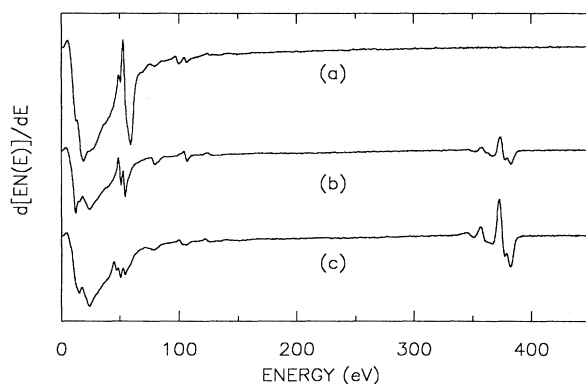

FIG. 5. Auger data showing the regrowth of GaN on a Ni film (deposited on GaN) by reaction of a Ga metal overlayer with outdiffusing N (see text). All spectra are on the same vertical scale with a 2-eV pp modulation. (a) Ni/GaN ($\Theta_{Ni} \approx 90$) after a 20-sec anneal at 900 °C. In the high-energy region (not shown) the (Ga 1070 eV)/(Ni 848 eV) PPH ratio is ~0.4, as in Fig. 4. (b) The same as (a) after deposition of a thick Ga film near room temperature followed by a 10-sec anneal at 800 °C. In the high-energy *LMM* region (not shown) little or no Ni is seen (Ni/Ga PPH ratio <0.05). (c) The same as (b) after a further 5-min, 950 °C anneal. In the high-energy *LMM* region (not shown) little or no Ni is seen (Ni/Ga PPH ratio <0.08).

4. Thermodynamic considerations

It is worthwhile to consider briefly the thermodynamic factors governing the interfacial reaction. The formation of GaN is reported[23] to be exothermic by $\Delta H = -26.4$ Kcal/mole. Nogami *et al.*[24] estimate $\Delta H \approx -0.38$ eV/atom (8.8 Kcal/mole) for the formation of a dilute solution of Ga in Ni. Nitrogen is found[17] to be essentially insoluble in solid or liquid Ni, but Conrad *et al.*[16] estimate $\Delta H \approx -135$ Kcal/mole for the heat of adsorption of atomic N on Ni(111). Hence $\Delta H \approx -117$ Kcal/mole is estimated for the reaction Ni+GaN→Ni[Ga] +Ni(N)$_{ads}$ (where "Ni[Ga]" means "a dilute solution of Ga in Ni" and "Ni(N)$_{ads}$" refers to "N adsorbed on Ni"). The driving force for the reaction thus derives mainly from the high stability of the bond between the Ni surface and atomic N. This result suggests an explanation for the fact, noted above, that rapid reaction does not occur until a sufficiently high temperature is reached to promote diffusion of free Ga away from the reaction zone which then allows interaction between Ni and GaN and the release of "free" N.

B. LEED

Figure 6 shows LEED results for the clean (0001)-(1×1) surface and for a similar surface after deposition of a thin ($\Theta_{Ni} \approx 6$) Ni layer followed by a 10-sec anneal at 900 °C. The initial Ni deposition near room temperature (not shown) results in a deterioration of the (1×1) pattern (i.e., increasing diffuse background) indicating growth of a disordered layer.

Annealing restores the (1×1) symmetry of the clean surface with, however, the appearance of an additional set of beams at a larger diffraction angle. This indicates coalescence of the thin Ni layer into islands. The outer spot of each pair arises from (111)-oriented crystalline Ni islands, in registry with the GaN(0001) substrate, and the inner spot from the relatively Ni-free GaN areas between islands (see below). Further deposition of a few monolayers of Ni near room temperature, on the surface giving Fig. 6(b), results in a rapid fading of the inner set of spots with the continued existence of the Ni(111)-(1×1) pattern (outer set of spots). As shown in Fig. 6(c), the Ni pattern persists during deposition of much thicker layers.

These results indicate that the ordered islands serve to nucleate subsequent growth of a thick crystalline Ni layer, in registry with the GaN, without further annealing. In comparison to the clean substrate, the thick Ni layer exhibits LEED spots which are somewhat more diffuse, and, in principle, the ordering could be improved by subsequent annealing. However, at the temperatures necessary for annealing of bulk Ni ($T \geq 700$ °C), reaction at the Ni/GaN interface is pronounced (Fig. 4).

Figure 7 shows schematic diagrams of the GaN(0001)-(1×1) and Ni(111)-(1×1) surfaces. The GaN and Ni primitive surface unit cells have lattice constants of $a = 3.18$ and 2.49 Å, respectively. The distance d from a LEED spot to the (0,0) is proportional to $\sin\theta$, where θ is the diffraction angle. Hence, for the spots in a given pair [Fig. 6(b)], the relationship $d_{GaN}/d_{Ni} = a_{Ni}/a_{GaN}$ should
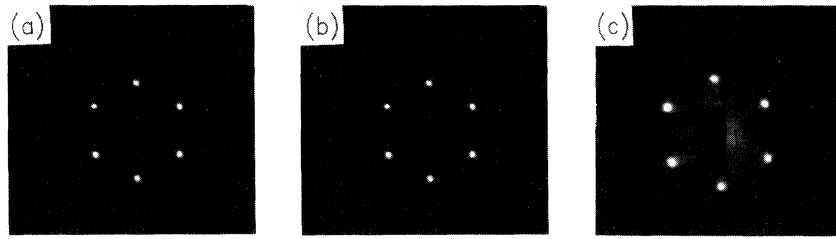
FIG. 6. LEED results for different surface treatments. In each case, E_p is the primary beam energy. Patterns (a) and (c) were obtained for one sample and (b) for another; hence (b) appears rotated by 30°. (a) Clean GaN(0001)-(1×1) ($E_p = 98$ eV). (b) The same as (a) after deposition of ~6 monolayers of Ni near room temperature followed by a 10-sec anneal at 900 °C ($E_p = 117$ eV). (c) The same as (b) after deposition of an additional ~85 monolayers of Ni near room temperature but without subsequent annealing ($E_p = 121$ eV).

apply. These two quantities, 0.78 and 0.783, respectively, are in excellent agreement.

Auger results given above, and other data discussed below, all indicate extensive intermixing of Ga and Ni during high-temperature annealing. It is thus somewhat surprising to observe the persistence of a Ni(111)-(1×1) LEED pattern after a 900 °C anneal [Fig. 6(b)]. However, as noted previously, Ga is soluble[17] in Ni up to a concentration of 28 at. % Ga. Conversely, the existence of the Ni(111)-(1×1) LEED pattern indicates that the Ga concentration does not exceed 28 at. % under these conditions. This may result from the competition between the rate of Ga desorption at the Ni surface and the rate of Ga supply by reaction at the interface.

Finally, as noted in Fig. 4, high-temperature annealing causes the appearance of Ga near the surface of the thick crystalline Ni layer. This is accompanied by formation of the Ga-induced superstructures shown in Fig. 8. For a 10-sec anneal at 700–800 °C a $(\sqrt{3} \times \sqrt{3})R 30°$ pattern appears. Annealing at ~900 °C leads to the replacement of this pattern by a weaker (2×2). In either case, the new structure may coexist with the Ni(111)-(1×1) on Ga-free areas of the surface (if any). The same two structures have been reported[25] for Si or Ge adsorbed on Ni(111) by SiH_4 or GeH_4 decomposition. Although specific models have not been proposed, the Si or Ge is thought[25] to be adsorbed at three-fold hollow sites.

C. ELS

Figure 9 shows surface-sensitive ELS data ($E_p \approx 100$ eV) for clean GaN(0001)-(1×1) and for thick Ni and Ga films. The assignment of structure in the Ni and Ga spectra has been discussed previously (Refs. 26 and 27, respectively), and the data in Fig. 9 are seen to be in good agreement with these results (after numerically differentiating to obtain $-d^2[EN(E)]/dE^2$ for comparison with published spectra). The GaN ELS has been discussed by Troost et al.[4] with reference to data for an Ar^+-ion bombarded (0001) surface. The present results, for an ordered surface, show similar but more highly resolved structure.

Figure 10 shows ELS data for the annealing of a thick Ni film on GaN(0001)-(1×1). Segregation of Ga to the surface during annealing (Fig. 4) leads to the appearance

of loss features associated with Ga atoms, particularly the Ga $3d$ excitation[4] near 20 eV. However, the metallic Ga surface and volume plasmons[27] ($\hbar\omega_s = 10.5$ and $\hbar\omega_p = 14.5$ eV, Fig. 9) are not observed. This suggests that the near-surface Ga is present in the form of isolated atoms or small clusters in the Ni matrix rather than as macroscopic, metallic Ga islands.

D. UPS

To obtain further insight concerning the initial formation of the Ni/GaN interface, a technique is required which can distinguish different chemical forms of Ga and which is also highly surface specific. The low-energy Auger spectrum (Fig. 1) cannot easily be used for this purpose because of the overlap between the Ni and Ga transitions. Hence Ga $3d$ photoemission data have been recorded using Zr $M\zeta$ excitation ($h\nu = 151.4$ eV). The resulting Ga $3d$ photoelectrons, with a kinetic energy of ~126 eV, have a minimal IMFP and are well separated from any strong Auger features (Fig. 1). The results are shown in Fig. 11, and the data reduction procedure used to analyze the raw spectra is summarized in Appendix B.
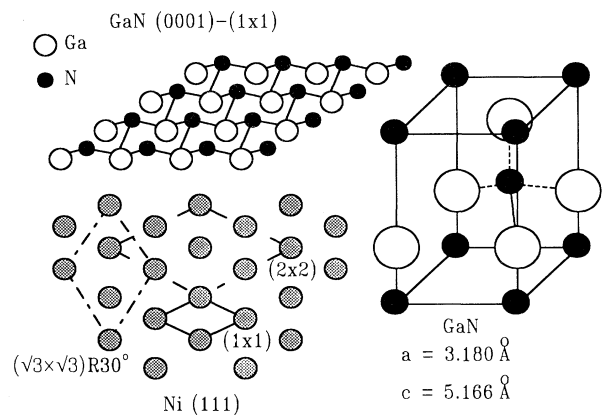

FIG. 7. Schematic diagram (not to scale) of the N-terminated GaN(0001)-(1×1) surface. Other diagrams show the wurtzite (ZnO) unit cell of GaN and the (111) surface geometry of crystalline (face-centered cubic) Ni. Primitive unit cells are shown for (1×1), $(\sqrt{3} \times \sqrt{3})R 30°$, and (2×2) structures (see text).
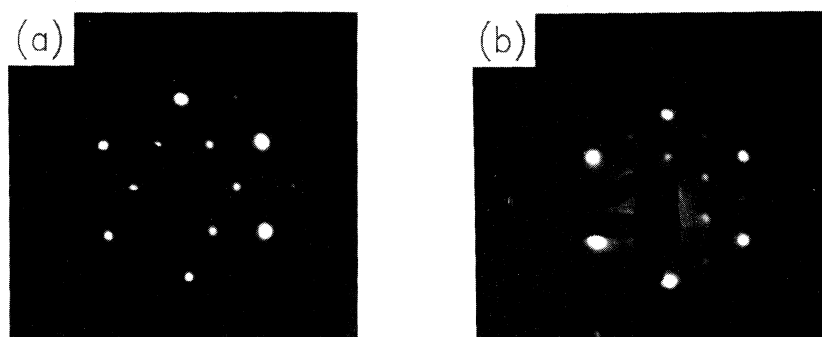
FIG. 8. LEED patterns appearing after annealing-induced segregation of Ga to the surface of a thick, crystalline Ni(111) layer on GaN(0001). (a) $(\sqrt{3} \times \sqrt{3})R\,30°$, after a 10-sec anneal at 800 °C ($E_p = 97$ eV). (b) (2×2), after 10-sec anneal at 900 °C ($E_p = 107$ eV), overexposed to show the weak fractional-order spots.

The purpose of the analysis described in Appendix B is to obtain estimates of the relative binding energies and intensities of overlapping features.

Figure 11(a) shows the clean GaN Ga $3d$. In comparison with data[2] obtained at a higher photon energy (Al $K\alpha_{1,2}$, $h\nu = 1486.6$ eV), there is no indication of a weak N $2s$ peak at ~ 3 eV higher kinetic energy. This results from the relatively low cross section[28] for s-electron photoionization at lower photon energies. Deposition of Ni near room temperature, Fig. 11(b), leads to a shoulder at higher kinetic (lower binding) energy. Annealing, Fig. 11(c), causes a shift to higher energy but little or no change in the intensity of the shoulder (about 0.16) relative to the main peak.

Previous XPS and UPS data for GaN (Refs. 2 and 3) and Ga metal[29] indicate a shift of 1.0–1.1 eV to higher kinetic energy for the metallic Ga $3d$ peak, and a further ~ 0.2-eV shift is observed[24] for a dilute solution of Ga in Ni. The resultant 1.2–1.3-eV shift is in reasonable agreement with the 1.7-eV shift of the shoulder in Fig. 11(c) relative to the main (unreacted GaN substrate) peak. Thus a strong chemical effect occurs at the immediate Ni/GaN interface formed at room temperature, leading to the release of "free" Ga. With annealing, a more extensive intermixing occurs. These results further indicate, as noted above, that the (1×1) LEED pattern shown in Fig. 6(b) arises not from pure Ni but from a solution of Ga in Ni.

The discussion thus far has been entirely in terms of relative kinetic (or, equivalently, relative binding) energies, avoiding any mention of absolute binding energies (BE's). For the clean GaN surface we obtain a Ga $3d$ BE of 20.6 ± 0.2 eV below the Fermi level, somewhat larger than the previously reported[2,3] value of 19.7 eV. However, upon successive depositions of a few monolayers of Ni, the BE of the unreacted substrate $3d$ peak (the main peak in each of the spectra in Fig. 11) shifts to 19.6 eV. For comparison, we obtain a BE of 18.6 eV for the $3d$ level of a thick Ga metal film (not shown), in close agreement with the result (18.7 eV) of Su et al.[29] for the centroid of the resolved $3d_{3/2}$-$3d_{5/2}$ doublet.

There are three possible explanations for the high Ga $3d$ BE on the clean GaN surface and the ~ 1.0-eV shift to lower BE with Ni deposition. One would be charging of the sample to a small positive potential due to photo-

electron emission and a finite surface conductivity. Deposition of a few monolayers of Ni might be sufficient to eliminate such charging. A second possibility would be differences in band bending among the samples used in various studies. In the present work, valence-band UPS data (not shown) indicate the Fermi level to be near midgap, (i.e., there is substantial upward band bending at the surface). However, a similar degree of band bending was observed by Hedman and Mårtensson,[2] who reported a ~ 0.9-eV smaller Ga $3d$ BE. Hence it appears that band bending alone cannot account for the Ga $3d$ BE differences. A third possibility is that radiation from the UPS excitation source induces a photovoltage effect by exciting electron-hole pairs, thus causing a decrease in the upward band bending (and a concomitant increase in Ga $3d$ BE) on the clean surface. A thin Ni overlayer (or contaminants remaining from the surface preparations in Refs. 2 and 3) might enhance surface recombination, thus reducing the photovoltage shift and bringing the Ga $3d$ to the "correct" BE of ~ 19.6 eV.
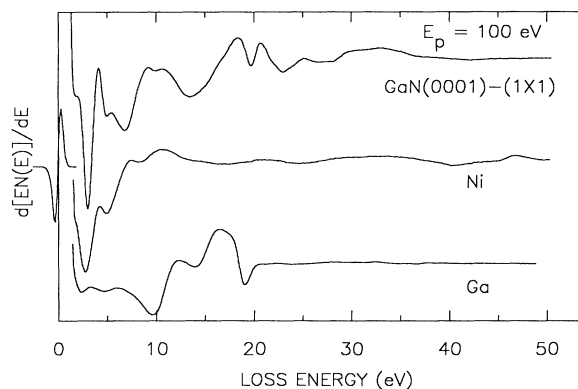

FIG. 9. Surface-sensitive ELS data (primary beam energy $E_p = 100$ eV) for clean GaN(0001)-(1×1) and for thick Ni and Ga films. The elastic peak is shown, on a reduced vertical scale, at the zero of loss energy. The relative magnitudes of different spectra are not quantitative. The weak structure in the Ni spectrum at 40–50-eV loss energy (60–50-eV kinetic energy) is due to the $M_{2,3}VV$ Auger transition.
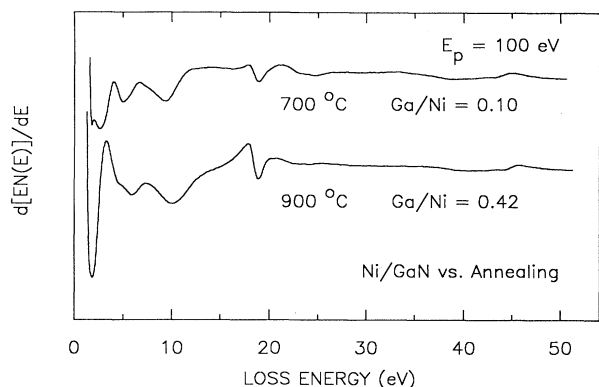
FIG. 10. ELS data, similar to Fig. 9, for the annealing of a Ni film ($\Theta_{Ni} \approx 90$) on GaN(0001)-(1×1). The (Ga 1070 eV)/(Ni 848 eV) PPH ratios are given. Each anneal was for ~10 sec at the indicated temperature. The relative magnitudes of the two spectra are not quantitative.

E. Model for Ni/GaN(0001)-(1×1) interface formation

This section summarizes our main results and conclusions.

(1) On a clean GaN surface, Ni deposited near room temperature grows in a layer-by-layer (Frank–van der Merwe) mode, as shown by the dependence of the Ni *LMM* Auger intensity on Θ_{Ni} (Fig. 3). The unannealed film is disordered.

(2) Annealing a thin Ni layer (a few monolayers) leads to formation of crystalline, (111)-oriented Ni islands in registry with the GaN (Fig. 6). During subsequent depo-
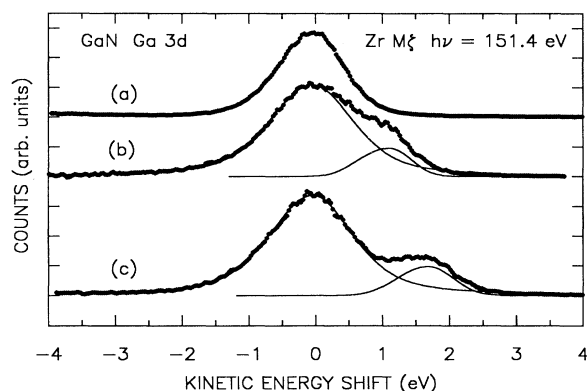

FIG. 11. Ga 3*d* UPS data for Ni/GaN(0001)-(1×1). (a) Clean GaN. (b) After deposition of ~7 monolayers of Ni near room temperature. (c) After a 10-sec anneal at 800 °C. The points (heavy lines) are the recorded spectra after processing, and the curves (light lines) are the results of least-squares fits (see text). Spectra (b) and (c) have been shifted to align the respective "unreacted" Ga 3*d* components with that of the bare surface. Relative intensities of different spectra are not quantitative.

sition of Ni near room temperature, these islands serve to nucleate the continued growth of a crystalline film without further annealing.

(3) Chemical reaction at the interface between GaN and Ni occurs even near room temperature (Figs. 4 and 11). The N released appears near the Ni surface, while the free Ga remains near the interface where it may impede further reaction at room temperature. Annealing a thick Ni layer above ~600 °C leads to a pronounced interfacial reaction, indicated by large N_2 pressure bursts and the appearance of Ga at the Ni surface (Figs. 4 and 10).

(4) Upon intermixing, the Ga remains dissolved in the Ni rather than forming a surface-segregated layer or a stable Ni-Ga compound. ELS (Fig. 10) does not show metallic Ga surface or bulk plasmons, and LEED (Figs. 6 and 8) continues to show strong Ni(111)-(1×1) diffraction. Diffraction patterns are also seen indicating either $(\sqrt{3} \times \sqrt{3})R\,30°$ or (2×2) Ga-induced superstructures, depending on annealing temperature.

(5) A thick layer of metallic Ga vapor-deposited on a thick Ni film is able to recombine, during subsequent annealing, with the free nitrogen escaping through the Ni layer (Fig. 5). After desorption of the unreacted Ga, a poorly ordered layer of GaN remains.

ACKNOWLEDGMENT

APPENDIX A

This appendix describes the approach used to estimate the coverage of adsorbed impurities, such as C and O, from Auger intensities. It is assumed that the substrate is GaN(0001), terminated in a monolayer of N, and that no intermixing occurs, i.e., that the adsorbate is bonded above the outermost layer of substrate atoms.

The first-derivative Auger peak-to-peak heights for adsorbate X and for substrate N atoms are given by

$$I_X = \alpha \sigma_X S_X ,$$

$$I_N = f \alpha \sigma_N S_N \sum_{n=0}^{\infty} \exp(-nd/\lambda \cos\phi) ,$$

where α is an instrumental scale factor depending on primary beam current, CMA transmission, detection system gain, etc. Any dependence of α on Auger electron energy is assumed to be small over the range of interest and to be included implicitly in the relative atomic sensitivities (see below). The quantity $f \le 1$ accounts for the (small) attenuation of the N AES signal by the adsorbate layer. The quantities σ_X and σ_N are, respectively, the numbers of adsorbate and N atoms per cm^2, with the coverage being defined as $\Theta_X = \sigma_X / \sigma_N$. The *atomic* Auger sensitivities for $E_p = 3$ keV, S_X and S_N, are obtained from the tabulated elemental sensitivities as described by Payling.[30] The above expressions neglect corrections to S_X and S_N due to differences in electron backscatter between GaN and the reference compounds from which the elemental

sensitivities are obtained[30] (e.g., Si nitride for N and MgO for O). In the wurtzite GaN lattice (Fig. 7), layers of N are spaced along the c axis by $d = 2.583$ Å. The electron IMFP, estimated following Tanuma, Powell, and Penn,[13] is $\lambda \approx 9.6$ Å in GaN at the N KLL energy of 380 eV. Finally, $\phi = 42°$ is the CMA collection angle.

Evaluating the sum numerically (for $f = 1$, i.e., small Θ_X), one obtains $\Theta_X \approx 3.26(I_X/I_N)(S_N/S_X)$ at $E_p = 3$ keV, where I_N and S_N pertain to the main N KLL peak at ~380 eV.

APPENDIX B

In this appendix, the procedure used to analyze the Ga $3d$ UPS is briefly summarized. The general approach has been discussed by several authors, e.g., Refs. 31, 32, and works cited.

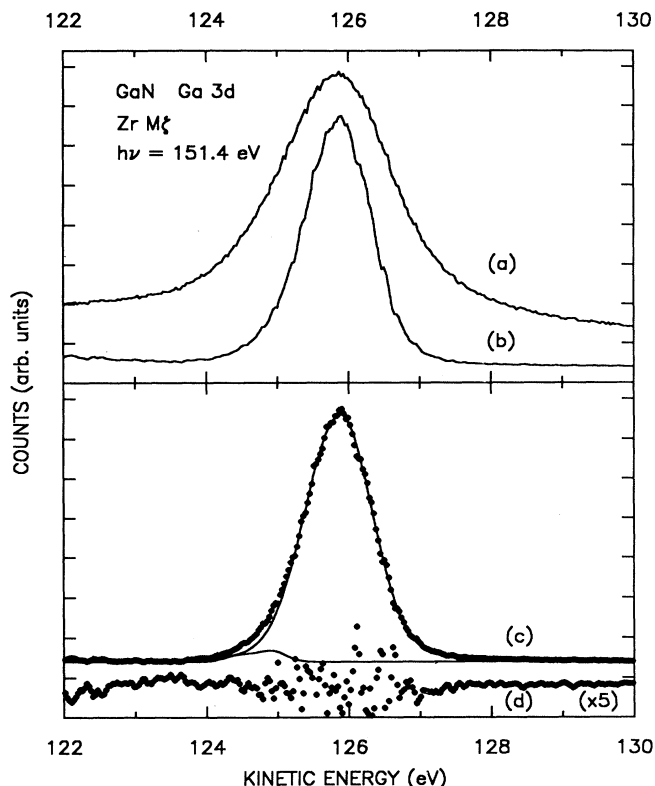The raw spectrum, Fig. 12(a), is first subjected to poly-

FIG. 12. Ga $3d$ UPS results illustrating the data-reduction sequence described in the text. Data for an oxygen-contaminated surface have been used to show the detection of a weak oxide satellite in the Ga $3d$ spectrum. (a) Raw data. (b) After polynomial smoothing, subtraction of the background due to inelastic scattering of higher-energy primary electrons and iterative deconvolution of a Lorentzian representing the Zr $M\zeta$ emission. (c) Results of least-squares fitting (b) with a sum of Gaussian-broadened Lorentzians (solid curves) and a background function (see text). The points show the data in (b) after removal of this background. (d) Spectrum of "residuals" (data minus fit), multiplied by a factor of 5, indicating the absence of a significant systematic error in the fit.

nomial (Savitzky-Golay) smoothing and a background, arising from inelastic scattering of primary electrons at higher kinetic energy, is subtracted. For the case at hand, these higher-energy primaries consist of photoelectrons and Auger electrons excited by the 2042.2-eV $L\alpha_{1,2}$ line in the Zr emission as well as valence-band electrons excited by the $M\zeta$ line. This background, which is assumed to be slowly varying over the narrow Ga $3d$ energy range, is obtained from a linear fit to the data at energies just above the high-energy tail of the Ga $3d$. Next, a Lorentzian representing the Zr $M\zeta$ line[33,34] is iteratively deconvoluted[31] from the data using the van Cittert ratio method. The result, shown in Fig. 12(b), is then used as input to the least-squares fitting routine.

Each chemically distinct Ga $3d$ band is modeled by a pair of Gaussian-broadened Lorentzian (Voigt) functions representing the $3d_{3/2}$ and $3d_{5/2}$ spin-orbit components. The splitting and branching ratio, which are not expected to be chemically sensitive, are fixed at 0.45 eV and 0.61, respectively, as reported[35] for high-resolution GaAs Ga $3d$ spectra. The analytic approximation to the Voigt function described by Wertheim et al.[36] is used, and the energy, intensity, total width, and degree of Gaussian broadening are unconstrained in the fit. The Gaussian width represents "solid-state effects" such as phonon and inhomogeneous broadenings in the sample; the CMA resolution width (~0.4 eV) is small compared to the linewidths in Figs. 11 and 12.

Included in the fit is a function representing the background near the low-kinetic-energy side of the Ga $3d$ peak. For a metallized (e.g., Ni-covered) surface this background is due to inelastic scattering of the Ga $3d$ photoelectrons and is modeled using the semiempirical scattering function described by Tougaard[37] and by others.[38] For the clean GaN surface, inelastic scattering is not significant for loss energies less than the band gap ($E_g = 3.39$ eV, Ref. 1). (This assumption is valid if surface and/or defect states in the gap do not provide a significant loss channel). The background intensity, which is much less in this case, arises from a small non-linear contribution not removed by the linear subtraction described above and is modeled using a second-order polynomial. In either case, the background parameters are unconstrained in the least-squares fitting.

One criterion for a good fit[39] is that the spectrum of "residuals," i.e., a plot of fit minus data, show only random noise. Attempts to fit the data in Fig. 12(b) with a single Ga $3d$ doublet (not shown) resulted in structure near 125 eV indicating a systematic error. Inclusion of a second Ga $3d$ doublet in the fit produced the results in Figs. 12(c) and 12(d). The surface giving these data was (intentionally) oxygen contaminated, with a coverage of $\Theta_0 \approx 0.05$ monolayers estimated as in Appendix A. The position of the weak satellite, ~0.8 eV to higher binding energy from the GaN Ga $3d$, is within 0.1 eV of the value expected for Ga oxide as observed[29] for O_2 chemisorption on Ga metal. A second criterion[39] is that none of the parameter correlation coefficients approach unity in magnitude. For the results shown in Figs. 11 and 12, none of these quantities exceed 0.85 which, as discussed in Ref. 39, indicates reasonably good fits.

One final comment concerns the choice of line shape used in the fit. A Lorentzian line shape is appropriate only to nonmetallic systems. For metals, simultaneous excitation of core- and Fermi-level electrons results in an asymmetric, Doniach-Sunjic (DS) line shape;[32] hence a Gaussian-broadened DS function should be used to represent the Ga $3d$ of Ga dissolved in Ni (Fig. 11). However, the Ga $3d$ UPS of a thick Ga metal film (not shown) exhibits only a small DS asymmetry, so only Voigt functions were used in the fits shown in Fig. 11.

[1]S. Strite and H. Morkoç, J. Vac. Sci. Technol. B **10**, 1237 (1992).

[2]J. Hedman and N. Mårtensson, Phys. Scr. **22**, 176 (1980).

[3]R. Carin, J. P. Deville, and J. Werckmann, Surf. Interface Anal. **16**, 65 (1990).

[4]D. Troost, H.-U. Baier, A. Berger, and W. Mönch, Surf. Sci. **242**, 324 (1991).

[5]L. A. DeLouise, J. Vac. Sci. Technol. A **10**, 1637 (1992).

[6]X.-Y. Zhu, M. Wolf, T. Huett, and J. M. White, J. Chem. Phys. **97**, 5856 (1992); X.-Y. Zhu, T. Huett, M. Wolf, and J. M. White, Appl. Phys. Lett. **61**, 3175 (1992).

[7]M. A. Khan, J. N. Kuznia, D. T. Olson, and R. Kaplan, J. Appl. Phys. **73**, 3108 (1993).

[8]É. S. Kopeliovich, V. N. Maslov, V. Yu. Pepelyaev, V. N. Rukova, V. G. Sidorov, M. D. Shagalov, and Yu. K. Shalabutov, Fiz. Tekh. Poluprovodn. **9**, 183 (1975) [Sov. Phys. Semicond. **9**, 125 (1975)].

[9]M. A. Khan, J. N. Kuznia, J. M. Van Hove, D. T. Olson, S. Krishnankutty, and R. M. Kolbas, Appl. Phys. Lett. **58**, 526 (1991).

[10]H. P. Steinrück, M. P. D'Evelyn, and R. J. Madix, Surf. Sci. **172**, L561 (1986).

[11]R. Vanden Berghe and R. Vlaeminck, Surf. Interface Anal. **10**, 316 (1987).

[12]S. Z. Weisz, M. Gomez, O. Resto, A. Many, and Y. Goldstein, Surf. Interface Anal. **19**, 264 (1992).

[13]S. Tanuma, C. J. Powell, and D. R. Penn, Surf. Interface Anal. **17**, 911 (1991); **17**, 927 (1991).

[14]Y. Shapira and D. Lichtman, in *Methods of Experimental Physics Vol. 14—Vacuum Physics and Technology*, edited by G. L. Weissler and R. W. Carlson (Academic, New York, 1979), p. 345.

[15]S. Dushman, *Scientific Foundations of Vacuum Technique*, 2nd ed. (Wiley, New York, 1962), Chap. 1.

[16]H. Conrad, G. Ertl, J. Küppers, and E. E. Latta, Surf. Sci. **50**, 296 (1975).

[17]M. Hansen, *Constitution of Binary Alloys*, 2nd ed. (McGraw-Hill, New York, 1958); R. P. Elliot, *Constitution of Binary Alloys, First Supplement* (McGraw-Hill, New York, 1965).

[18]M. Ogawa, Thin Solid Films **70**, 181 (1980).

[19]T. Kendelewicz, R. Cao, K. Miyano, I. Lindau, and W. E. Spicer, J. Vac. Sci. Technol. A **7**, 749 (1989); T. Kendelewicz, M. D. Williams, W. G. Petro, I. Lindau, and W. E. Spicer, Phys. Rev. B **32**, 3758 (1985); M. D. Williams, W. G. Petro, T. Kendelewicz, S. H. Pan, I. Lindau, and W. E. Spicer, Solid State Commun. **51**, 819 (1984).

[20]E. Roman and R. Riwan, Surf. Sci. **118**, 682 (1982).

[21]M. Grunze, R. K. Driscoll, G. N. Burland, J. C. L. Cornish, and J. Pritchard, Surf. Sci. **89**, 381 (1979).

[22]Y. Kuwahara, M. Fujisawa, M. Onchi, and M. Nishijima, Surf. Sci. **207**, 17 (1988).

[23]D. D. Wagman, W. H. Evans, V. B. Parker, I. Halow, S. M. Bailey, and R. H. Schumm, *Selected Values of Chemical Thermodynamic Properties*, Natl. Bur. Stand. (U.S.) Technical Note No. 270-3 (U.S. GPO, Washington, D.C., 1968), p. 220.

[24]J. Nogami, T. Kendelewicz, I. Lindau, and W. E. Spicer, Phys. Rev. B **34**, 669 (1986).

[25]L. H. Dubois and R. G. Nuzzo, Surf. Sci. **149**, 133 (1985).

[26]K. Akimoto, Y. Sakisaka, M. Nishijima, and M. Onchi, Surf. Sci. **82**, 349 (1979).

[27]J. E. Rowe, G. Margaritondo, and S. B. Christman, Phys. Rev. B **15**, 2195 (1977).

[28]W. C. Price, A. W. Potts, and D. G. Streets, in *Electron Spectroscopy*, edited by D. A. Shirley (North-Holland, Amsterdam, 1972), p. 187.

[29]C. Y. Su, P. R. Skeath, I. Lindau, and W. E. Spicer, Surf. Sci. **118**, 248 (1982).

[30]R. Payling, J. Electron Spectrosc. Relat. Phenom. **36**, 99 (1985).

[31]D. D. Hawn and B. M. Dekoven, Surf. Interface Anal. **10**, 63 (1987).

[32]G. K. Wertheim and S. B. Dicenzo, J. Electron Spectrosc. Relat. Phenom. **37**, 57 (1985).

[33]M. O. Krause, Chem. Phys. Lett. **10**, 65 (1971).

[34]D. A. Allison and R. G. Cavell, J. Chem. Soc. Faraday Trans. 2 **72**, 118 (1976).

[35]T. Miller and T.-C. Chiang, Phys. Rev. B **29**, 7034 (1984).

[36]G. K. Wertheim, M. A. Butler, K. W. West, and D. N. E. Buchanan, Rev. Sci. Instrum. **45**, 1369 (1974). There is a typographical error in the definition of the quantity b, which should be $b = 1/[2\sqrt{\ln(2)}]$.

[37]S. Tougaard, Surf. Sci. **216**, 343 (1989).

[38]H. Tokutaka, N. Ishihara, K. Nishimori, S. Kishida, and K. Isomoto, Surf. Interface Anal. **18**, 697 (1992).

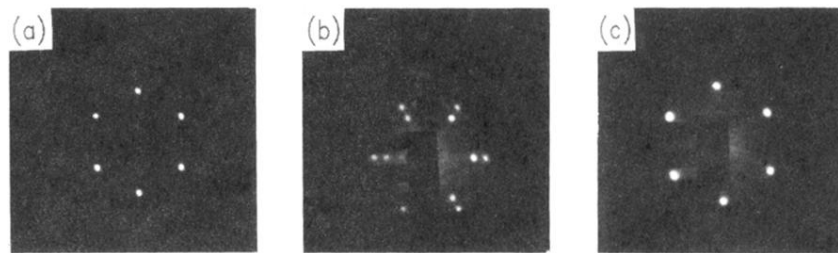[39]G. K. Wertheim, J. Electron Spectrosc. Relat. Phenom. **60**, 237 (1992).

FIG. 6. LEED results for different surface treatments. In each case, E_p is the primary beam energy. Patterns (a) and (c) were obtained for one sample and (b) for another; hence (b) appears rotated by 30°. (a) Clean GaN(0001)-(1×1) ($E_p = 98$ eV). (b) The same as (a) after deposition of ~6 monolayers of Ni near room temperature followed by a 10-sec anneal at 900 °C ($E_p = 117$ eV). (c) The same as (b) after deposition of an additional ~85 monolayers of Ni near room temperature but without subsequent annealing ($E_p = 121$ eV).
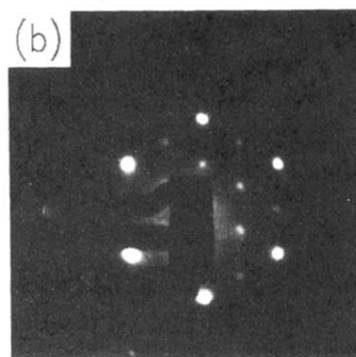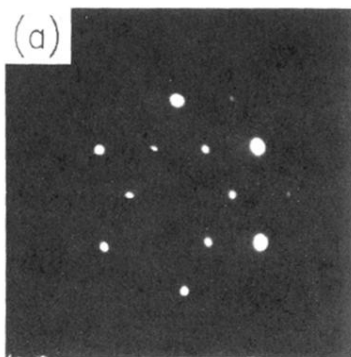
FIG. 8. LEED patterns appearing after annealing-induced segregation of Ga to the surface of a thick, crystalline Ni(111) layer on GaN(0001). (a) $(\sqrt{3}\times\sqrt{3})R\,30°$, after a 10-sec anneal at 800 °C ($E_p = 97$ eV). (b) (2×2), after 10-sec anneal at 900 °C ($E_p = 107$ eV), overexposed to show the weak fractional-order spots.